A Comparative Analysis of Partial Discharge in 13 Combined Insulation Structures of 11 Materials Used in Cast-Resin Dry-Type Transformers

Muzaffer Erdogan and Mehmet Kubilay Eker

***Abstract*— Partial discharge (PD) in cast-resin dry-type transformers (CRDTs) is an important issue that needs to be overcome. In this study, PD in insulation materials used in CRDT windings is investigated. Four types of samples are prepared using 11 different types of materials, including epoxy resin, three-ply glued polyester insulation, prepreg insulation, glass fiber mesh, polyester adhesive tape, polyester film, polyimide film, rectangular conductors with polyester insulation, round conductors with polyester insulation, round conductors with enamel insulation, and foil conductors without insulation, and subjected to PD measurements. The samples are placed into a mold for resin casting that is similar to those used to fabricate large cast-resin windings, and the material behavior is tested. PD measurements are carried out in the high-voltage laboratory of the BEST Transformer Company. The measured data are used as inputs to models of the samples that are simulated using finite element analysis software to determine the PD inception electric field. The PD patterns of the samples are compared with well-known PD patterns in the literature. Finally, a comparative analysis of the materials is performed, and strong and weak materials against PD are identified. The results of this study show that laminated insulation materials or fiberglass meshes, both with epoxy resin, which have PD inception at a mean value of 3.4 kV/mm of electric field intensity, are more susceptible to PD than the other insulation materials investigated. In contrast, insulated conductors or nonlaminated polyester or polyimide films, all with epoxy resin, which have PD inception above a mean value of 5.3 kV/mm of electric field intensity, are robust to PD.**

***Index Terms*— Cast-resin dry-type transformers (CRDTs), electric field simulation, insulation materials, partial discharge (PD), PD pattern.**

I. Introduction

A SCARCITY of natural resources has resulted in a rapid increase in energy requirements and an increase in the demand for efficient energy transfer. It is efficient to transfer electrical energy at a medium voltage (MV) in close proximity to the actual location of energy consumption. However, extra precaution and safety measures are required in highly populated areas. Furthermore, it is safer to use a cast-resin dry-type transformer (CRDT) than to use oil-based insulation and cooling media for energy delivery at a distribution network. In addition, dry-type transformers do not require maintenance because of a solid construction [1].

A CRDT winding structure consists of conductors separated by polyester-based laminated insulation, where groups of conductors are wrapped in resin-impregnated fiberglass mesh, and all the materials are encapsulated in an epoxy resin. However, partial discharge (PD) is a critical issue for CRDTs because of the solid winding structure. Voids that form within the insulation of the winding may be harmful and cause insulation failure [2]. In addition, cracks in the epoxy resin or delamination of insulation can occur inside the CRDT windings due to the different thermal expansion coefficients of the materials used [3]. To minimize the occurrence of PD in CRDT, the insulation materials used in the winding should be investigated.

A. Related Studies

Many PD studies on various winding and insulation types can be found in the literature. The PD inception voltage of an enamel conductor was investigated for twisted round conductor pairs and parallel-plate conductors with different insulation thicknesses and gaps [4]. The minimum PD inception voltage was obtained using a well-defined insulation thickness and a gap between conductors. Ozaki *et al.* [5] studied enamel conductors with different nanofillers and thicknesses. The high shearing force of the kneading process and a nanofiller content of up to 10 pbw were found to improve the breakdown time and flexibility of the insulation. Polymer materials with nanofillers were found to decrease the susceptibility to PD compared with polymers with microfillers [6]. Besides, the addition of titanium dioxide (TiO_2) into the low-density polyethylene (LPDE) matrix was found to decrease the PD activity compared with pure LPDE [7]. PD and surface tracking of LPDE with nanofillers of silicon dioxide (SiO_2), TiO_2 and TiO_2@SiO_2 have also been investigated [8]. The

Manuscript received 23 April 2022; revised 9 August 2022 and 28 August 2022; accepted 5 September 2022. Date of publication 8 September 2022; date of current version 27 December 2022. *(Corresponding author: Muzaffer Erdogan.)*

Muzaffer Erdogan is with the Department of Dry-Type Transformer Electrical Design, Best Transformer Company, 10100 Balikesir, Turkey (e-mail: muzaffer.erdogan@besttransformer.com).

Mehmet Kubilay Eker is with the Department of Electrical and Electronics Engineering, Balikesir University, 10145 Balikesir, Turkey (e-mail: kubilay@balikesir.edu.tr).

Color versions of one or more figures in this article are available at https://doi.org/10.1109/TDEI.2022.3205285.

Digital Object Identifier 10.1109/TDEI.2022.3205285

best results were obtained using TiO_2@SiO_2 with a 0.6% filler loading. Zhao *et al.* [9] performed experiments on epoxy resin and layer insulation materials, such as Nomex paper, dacron/mylar/dacron (DMD) material, polyester, and polyimide, to determine the surface PD and surface flashover at different high-frequency source voltages. Increasing the frequency was found to decrease the flashover voltage and affect the surface discharge inception. An artificial cavity was created within layers of Nomex paper and PD was measured [10]. With increasing voltage, the number of PD events and the magnitude of PD increased, the phase distribution broadened, and the phase of initial discharge moved forward. Moranda *et al.* [11] measured and compared the PD levels of Nomex paper and cellulose paper with different moisture contents in an oil cup. The PD inception voltage decreased significantly with increasing moisture. Florkowski *et al.* [12] investigated the change in the surface resistance after aging materials, such as cable insulating paper, epoxy-impregnated paper, machine insulation polyester film saturated with epoxy resin, and mica saturated with epoxy resin. Decreasing the surface resistance resulted in an increase in the inception voltage on the void surfaces after an aging period. The change in the dielectric properties of epoxy resin-impregnated paper was investigated from the initial stage of PD to the near-breakdown stage, and deterioration of the samples was explained [13]. Song *et al.* [14] analyzed that low temperatures increase charge trapping in a glass-fiber-reinforced epoxy resin, along with inducing excessive conduction and structural damage. Wang *et al.* [15] studied the aging of a fiberglass-reinforced epoxy resin at 130 °C for up to 32 days and found that PD after thermal aging causes a higher degree of molecular chain fracture than thermal aging or PD alone.

B. Motivation

MV windings control the lifespan of a dry-type transformer. These windings consist of conductors and many insulation materials that determine the insulation level in terms of PD and breakdown. The PD and breakdown properties of a single material or a combination of materials used in dry-type and oil-type transformers were evaluated in the aforementioned studies [4], [5], [9], [10], [11], [12], [14], [15]; however, sufficient information was not obtained to improve the insulation design of complex cast-resin winding. This study is motivated by the lack of studies in the literature on comparing combinations of materials used in cast-resin windings with similar structures.

C. Contributions

The objective of this study is to investigate insulation materials for cast-resin windings to obtain PD behavior in compliance with standards [16], [17]. PD behavior is investigated for a combination of conductor insulation, polymer insulation, and resin materials, which are the most commonly used insulation materials in cast-resin windings.

D. Organization

The remainder of this article is organized as follows. In Section II, sample preparation is detailed. In Section III, a PD measurement system is presented, including a detailed description of all the components. In Section IV, details of a simulation of the electric field in the samples are presented. To classify the PD patterns obtained in this study, similar patterns identified in the literature are given in Section V. In Section VI, the test results and finite element analyses for the electric field are presented. Finally, a discussion and concluding remarks are presented in Sections VII and VIII, respectively.

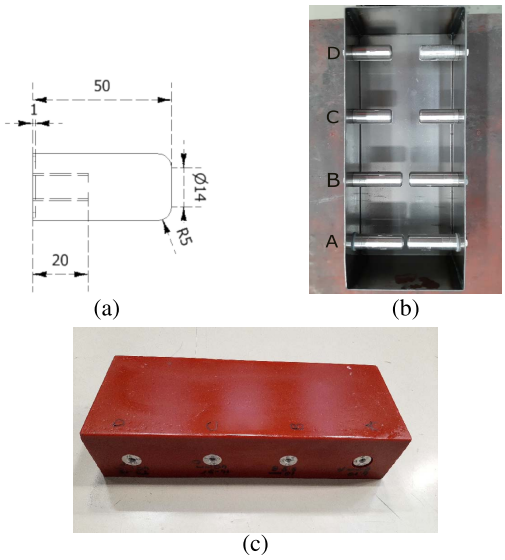

Fig. 1. Sample preparation. (a) Electrode dimensions. (b) Casting bucket with electrodes. (c) Cast samples.

II. Preparation of Samples

To investigate the PD states encountered in the components of a CRDT winding, samples are cast using aluminum electrodes placed in a steel bucket as a mold, as shown in Fig. 1. The diameter of the cylindrical aluminum electrodes is 24 mm, with a chamfer of 5 mm, as shown in Fig. 1(a). The bucket has eight holes through which four types of samples, labeled from *A* to *D*, are placed on the bucket walls, as shown in Fig. 1(b). The distances between the electrodes are adjusted by inserting aluminum spacers behind the main electrodes. Samples comprising electrodes, insulation materials, and conductors are prepared. Each mold is placed in a casting oven and maintained under vacuum for 2 h before starting the casting process. A mix is prepared using a mass ratio of epoxy (CY5538), hardener (HY 5571), and silica of 100:100:360 and subjected to vacuum degassing. Samples are cast under a vacuum to ensure no air bubbles remain. Then, the samples are cured for gelification at 80 °C for 8 h and for postcuring at 130 °C for 12 h, similar to the winding curing process. At the end of the curing process, the samples are demolded and prepared for testing, as shown in Fig. 1(c).

A detailed description of the materials used for sample preparation is given in Table I. These materials are used in actual cast-resin windings and are used for mass production of the BEST Transformer Company.

TABLE I
MATERIALS USED FOR SAMPLE PREPARATION

Code	Material	Width/Dia	Thickness	Insulation structure
R	Epoxy resin			Casting material, Type: Huntsman CY 5538 - HY 5571 - silica, ϵ_r: 4.3
C1	Conductor with insulation	5.5	1.8	Polyester, fiberglass string, varnish (thickness: 0.2), ϵ_r: 4.2
C2	Conductor with insulation	⌀2.1		Polyester, fiberglass string, varnish (thickness: 0.2), ϵ_r: 4.2
C3	Conductor with insulation	⌀2.1		Enamel (thickness: 0.05), ϵ_r: 4.3
C4	Conductor	40	0.5	Without insulation, ϵ_r: NA
L1	Insulation		0.31	Three-ply polyester film with glue, ϵ_r: 3.2
L2	Insulation		0.18	Three-ply polyester film with semi-cured resin, ϵ_r: 3.2
L3	Insulation		2.5	Fiberglass mesh with resin, ϵ_r: 4.4
L4	Insulation		0.05	Polyester adhesive tape, ϵ_r: 3.2
L5	Insulation		0.05	Polyester film, ϵ_r: 3.2
L6	Insulation		0.05	Polyimide film, ϵ_r: 3.4

*Dimensions are in mm.

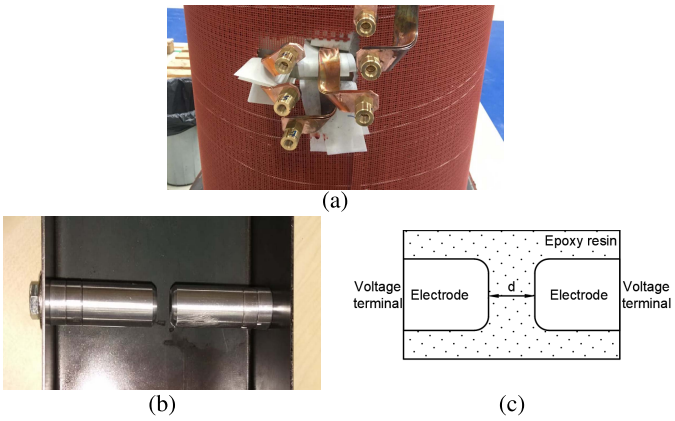

Fig. 2. Type-1 sample. (a) Bare conductors at the tapping area of a CRDT winding. (b) Sample before casting. (c) Diagram of the sample.

Samples are prepared to investigate various locations in cast-resin windings that are subjected to high potential differences. First, the tapping area in a cast-resin winding is considered. For voltage regulation, conductors are placed at a specific number of turns of the winding and connected to bolts before casting. The potential difference between the taps can increase up to 7.5 kV. These tap conductors are bare, there is no extra insulation material between conductors, as shown in Fig. 2(a), and an epoxy resin fills all the available space during casting. Type-1 samples are prepared with the aforementioned structure. The casting bucket only contains electrodes separated by a distance of d, as shown in Fig. 2(b), and the resin mix is cast. A diagram of a Type-1 sample is presented in Fig. 2(c).

The configurations of Type-1 samples are given in Table II, along with the distances between the electrodes. The samples are prepared following the specifications given in this table. Four samples are prepared for each casting in the bucket. The number of the sample label indicates the casting order, and the letter of the sample number indicates the location of the sample in the bucket, as shown in the No column of Table II. After casting Type-1 samples, Samples 4A and 6A are reproduced similar to the previous samples to check whether the casting quality is the same as for casting orders 1 and 2.

Uninsulated foil conductors are widely used in the MV windings of cast-resin transformers in the power range of

TABLE II
CONFIGURATIONS OF TYPE-1 SAMPLES

No	Material	d(mm)
1A	R	8.48
1B	R	8.8
1C	R	8.93
1D	R	9.22
2A	R	2
2B	R	3
2C	R	4
2D	R	5
4A	R	5
6A	R	4.1

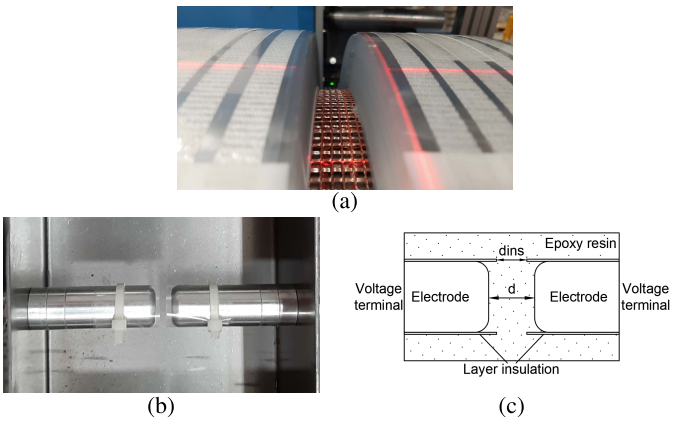

Fig. 3. Type-2 sample. (a) Winding with a foil conductor. (b) Sample before casting. (c) Diagram of the sample.

630–4000 kVA in the BEST Transformer Company. The conductors range from 30 to 200 mm in width and from 0.2 to 2.5 mm in thickness. An MV winding with an uninsulated foil-type conductor with layer insulation is shown in Fig. 3(a). A layer of insulation larger than the conductor width is placed between turns, and the space between adjacent disks is filled during casting. A high-voltage potential difference of up to 2 kV occurs in the insulation between the disks. Type-2 samples have a similar structure and consist of a pair of electrodes wrapped by insulation materials, such as polyester film, polyimide film, three-ply polyester, three-ply prepreg polyester, fiber adhesive tape, and fiberglass mesh, as shown in Fig. 3(b). The distance d between the electrodes and the

TABLE III
MATERIAL CONFIGURATIONS OF TYPE-2 SAMPLES

No	Material	d(mm)	d_{ins}(mm)
3B	R+L3	15	10
4B	R+L1	15	0
4C	R+L1+L4	16	0
4D	R+L2	15	0
5C	R+L1	6	0
6B	R+L5	8.8	4
6D	R+L6	9	4
8A	R+L3	15	10
8B	R+L1	10	0
9A	R+L1	8	0
9B	R+L1	7	0
10A	R+L3	7	0
11A	R+L1+L4	10	0
11B	R+L1+L4	10	0

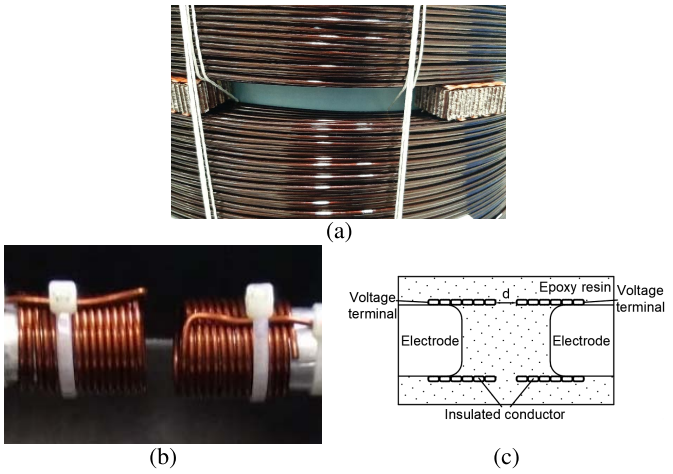

Fig. 4. Type-3 sample. (a) Winding with an enamel-insulated round conductor. (b) Sample before casting. (c) Diagram of the sample.

distance d_{ins} between the insulation materials are set during sample preparation, as shown in Fig. 3(c).

The configurations of Type-2 samples are given in Table III, along with the distances between the conductor components and between the insulation materials. The electrodes are completely wrapped in insulation, where d_{ins} equals 0 mm. In this case, small holes are made in the insulation materials to ensure resin filling between the electrodes and insulation materials.

Transformers with a 36-kV voltage winding and less than 2.5 MVAs are produced using the enamel or fiberglass-insulated round and rectangular conductors that are used in BEST Transformer Company. The conductors are used in an MV winding with a low current rating, and layer insulation is not required because of the winding structure. The winding can be separated into internal groups, as shown in Fig. 4(a), and the potential difference between the groups can reach up to 10 kV depending on the design. Type-3 samples have a similar structure and are prepared using insulated conductors. Electrodes are only used to keep the conductors inside the bucket. The conductors are wrapped around the electrodes, as shown in Fig. 4(b), maintaining a small gap d, as shown in Fig. 4(c). The distance between electrodes is larger than d to eliminate the electrode effect. The conductor leads are placed outside the bucket to apply the test voltage.

TABLE IV
MATERIAL CONFIGURATIONS OF TYPE-3 SAMPLES

No	Material	d(mm)
3A	R+C1	10
3C	R+C2	10
3D	R+C3	10
8C	R+C1	10
8D	R+C3	10

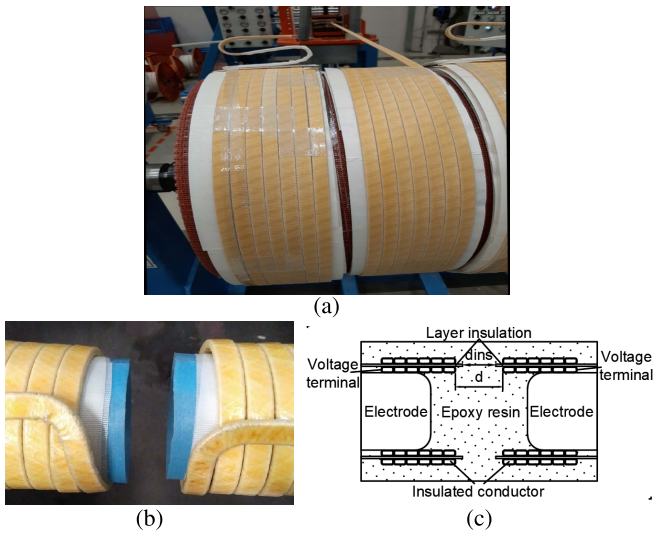

Fig. 5. Type-4 sample. (a) Cast-resin winding with an insulated conductor and layer insulation. (b) Sample before casting. (c) Diagram of the sample.

The configurations of Type-3 samples are given in Table IV, along with the distances between the conductor components.

Layer-type MV windings with many subwindings are often used to produce CRDTs above 4 MVA in the BEST Transformer Company. The conductors are insulated, and the insulation materials are used to separate the conductor layers, as shown in Fig. 5(a). A Type-4 sample is prepared to analyze this structure. Two conductor layers are wound around the electrodes to position the insulation material between the electrodes, as shown in Fig. 5(b). The conductor leads are placed outside the bucket to apply the test voltage. The distance d between the conductors is set, and the insulation material is placed between the conductor layers at a distance d_{ins}, as shown in Fig. 5(c).

The configurations of Type-4 samples are given in Table V, along with the distances between the conductor components and between the insulation materials.

III. PD MEASUREMENT SYSTEM

A PD measurement system is set up according to IEC 60270, where one test setup is shown in Fig. 6(a) and schematized in Fig. 6(b). In the diagram, U, Z, C_a, C_k, CD, CC, and MI denote the test voltage, filter, test sample, coupling capacitor, coupling device, connecting cable, and measurement instrument, respectively. PD measurements are carried out in the high-voltage laboratory of the BEST Transformer Company. The laboratory walls are surrounded by a Faraday cage. The voltage source is a single-phase high-voltage transformer

TABLE V
MATERIAL CONFIGURATIONS OF TYPE-4 SAMPLES

No	Material	d(mm)	d_{ins}(mm)
5A	R+C1+L1	13	5
5B	R+C1+L3	5	0
5D	R+C1+L3	10	0
6C	R+C4+L5	9	4
7A	R+C4+L5	10	5
7B	R+C4+L5	10	5
9C	R+C1+L1	6	0
9D	R+C1+L1	10	0
10D	R+C4+L6	9	4
11C	R+C1+L3	6	0
11D	R+C1+L1	5	0

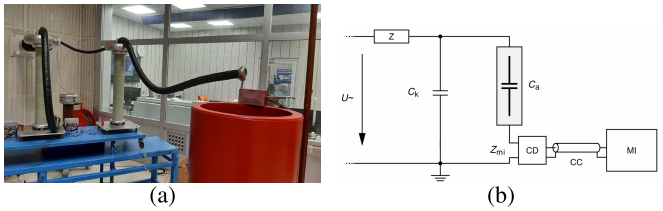

(a) (b)

Fig. 6. PD measurement system. (a) Test setup. (b) Schematized of the PD measurement system.

supplying voltages up to 36 kV without internal PD. C_k has a capacitance of 1 nF at a 100-kV insulation level. PD measurements are carried out using a CPL542 as the CD and an MPD600 PD analyzer as the MI, both of which are manufactured by Omicron [18]. Each test setup is calibrated with a 10-pC PD signal before performing measurements. The background noise of the laboratory is less than 5 pC. Each sample (C_a) is connected to the measurement equipment parallel to C_k, as shown in Fig. 6. During the tests, the applied voltage is increased from 0.9 to 36 kV in 100-V steps per second. All the PD measurements are recorded by the software of the PD system to facilitate detailed analysis.

IV. SIMULATION OF THE ELECTRIC FIELDS OF SAMPLES

Each sample has a different gap or material configuration. A comparative analysis of PD in the samples can be performed in terms of the electric field of PD inception. Therefore, finite element analysis software is used to model the electric fields of all the samples, as shown in Fig. 7. Finite element analysis divides the solution area into small triangles, which are voltage-distributed areas linearly, to minimize the energy in the solution area. When potential difference V is applied to electrodes, the energy w stored in the insulation medium region U between electrodes is given as [19]

$$w = \frac{1}{2}\int_U \epsilon \, |\text{grad}(V)|^2 dU. \tag{1}$$

PD inception voltage (V_{inc}) is applied to one electrode or conductor, and the other electrode or conductor is grounded. An axisymmetric model is used because the samples have a symmetrical structure. The solver precision in the finite element software is chosen as 10^{-8}. A triangular mesh with approximately 5000 nodes is used. The dielectric constants of the insulation materials are given in Table I.

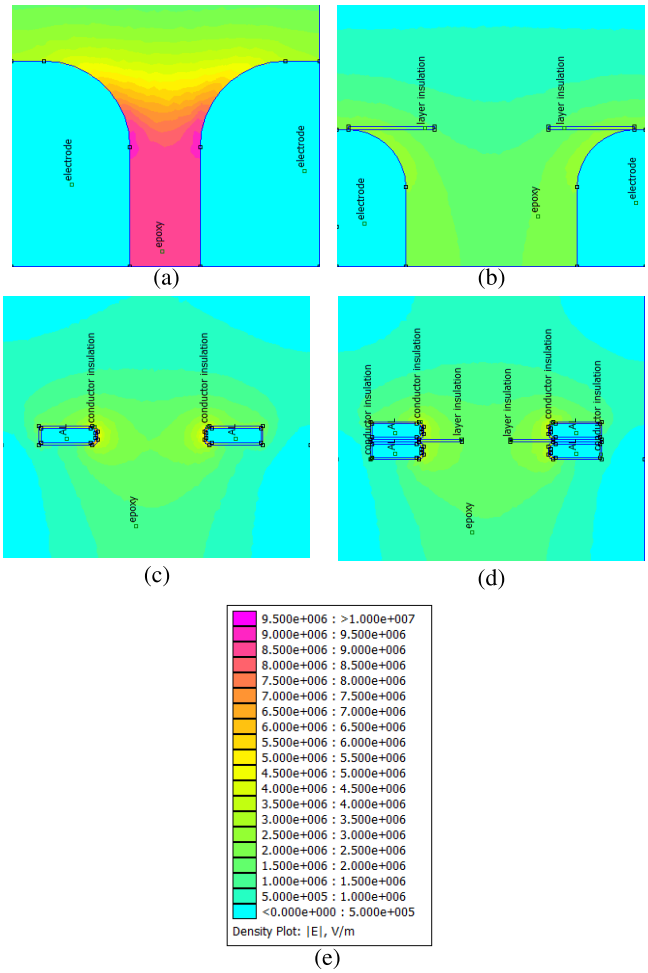

(a) (b) (c) (d) (e)

Fig. 7. FEM analysis of samples. (a) Electrodes: Type-1. (b) Electrodes with layer insulation: Type-2. (c) Conductor insulation: Type-3. (d) Conductors with layer insulation: Type-4. (e) Legend of simulation fields.

In the Type-1 sample, only epoxy resin is used as an insulation material. Therefore, the maximum electric field in the epoxy resin is determined, as shown in Fig. 7(a). The electric field in the layer insulation is analyzed for the model of the Type-2 sample, as shown in Fig. 7(b), and the electric field in the conductor insulation is analyzed for the model of the Type-3 sample, as shown in Fig. 7(c). The electric fields in both the conductor insulation and the layer insulation are investigated for the model of the Type-4 sample, as shown in Fig. 7(d).

V. PD PATTERNS IDENTIFIED IN THE LITERATURE

PD occurrence depends on many factors, such as the position, shape, and size of a void; the presence of floating conductor in the insulation materials; and the occurrence of a bad connection or corona. The recorded PD events show a unique pattern for each type of PD source [20], which can be used to identify the type of PD [21]. The PD source can be identified based on 16, 8, and 14 types of PD patterns presented in [20], [22], and [23], respectively. However, only four types of PD patterns are recorded during our experiments and discussed in this section. The PD results of the samples

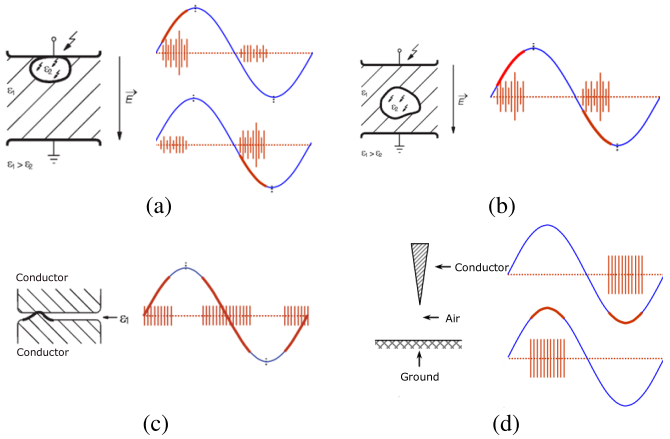

Fig. 8. Typical PD patterns [22], [23]. (a) Pattern-1: Direct contact between a void and an electrode. (b) Pattern-2: A void that does not contact an electrode. (c) Pattern-3: Bad contact. (d) Pattern-4: Corona.

are comparatively analyzed in Section VI using the typical PD patterns as shown in Fig. 8.

A void in the insulation medium is in direct contact with an electrode (Pattern-1) as shown in Fig. 8(a). Low-density high-amplitude PDs are observed at one-half of the voltage cycle, and high-density low-amplitude PDs are observed at the other half of the voltage cycle. For this type of PD, the ratio of the PD amplitudes between the half-cycles is at least three. If a void occurs near the electrode where the voltage is applied, low-density, high-amplitude PD events occur during the positive voltage cycle [22].

A void exists in the insulation medium that is not in contact with an electrode (Pattern-2) as shown in Fig. 8(b). Similar PD amplitudes and densities can be observed for both the half-cycles of the applied voltage; however, a ratio of up to 3:1 for the PD amplitudes in two half-cycles is normal [22].

Bad or loose contact of joint points between metallic connections of the test setup causes external PD events to occur outside the insulation medium, as shown in Fig. 8(c) (Pattern-3). PD with constant amplitude is recorded at the zero-crossing of the cycle. No PD is detected at the peak of the voltage cycle.

Fig. 8(d) shows a PD pattern for the corona at the sharp edge of the conductor component (Pattern-4). PD events occur externally in air, outside the solid insulation medium. The occurrence of PD in the negative half of the voltage phase indicates that there is a sharp edge on an electrode to which voltage is applied. The occurrence of PD in the positive half of the voltage phase indicates that there is a sharp edge on the ground side. PD occurs only at one-half the peak of the voltage cycle [22].

VI. Results

The results of the PD measurements and simulations for the samples are presented in this section, including the PD patterns.

A. Samples Containing Only Epoxy Resin (Type-1)

Table VI shows that no PD is recorded for all the Type-1 samples and maximum electric field in the epoxy medium for test voltages up to 30 kV. Although it is impossible in practice to prepare a resin mix that is completely bubble-free, voids may be sufficiently small that the amplitude of the resulting PD events is not detectable by the measurement system. To determine the maximum void size, Sample 6A is sliced and observed under a microscope. Many voids less than 8 μm in the insulation medium are found in the slice of Sample 6A. This result indicates that the pure resin mix produces undetectable PD events for electric fields up to 10 kV/mm, as shown in Table VI. However, the PD-free limit of the resin mix is accepted as 7.89 kV/mm for Type-2, Type-3, and Type-4 simulation evaluation, which is the second highest result, to strengthen this finding. As a result, only the electric field in the conductor and layer insulation is analyzed for Types-2–4 samples in Section VII. All the electric fields discussed below occur in the interior of the conductor insulation and layer insulation of the samples.

TABLE VI
Analysis Results of Type-1 Samples

Sample	Voltage$_{upto}$(kV)	PD	E$_{sim}$(kV/mm)
1A	30	None	4.35
1B	30	None	4.305
1C	30	None	4.23
1D	30	None	4
2A	20	None	10
2B	20	None	6.85
2C	20	None	5.3
2D	20	None	4.37
4A	25	None	5.6
6A	30	None	7.89

B. Samples With Layer Insulation (Type-2)

The recorded PD patterns of the Type-2 samples are shown in Fig. 9.

Fig. 9(a) shows two types of recorded PD patterns for Sample 3B. A PD pattern (red colored) similar to Pattern-3 is observed at the zero-crossing of the applied voltage. In addition, a low-density high-amplitude PD (blue colored) at the positive cycle and high-density low-amplitude PD (blue colored) at the negative cycle are recorded that are similar to Pattern-1.

Samples 4B and 4C exhibit PDs with similar shapes to that of Pattern-1, as shown in Fig. 9(b) and (c).

Fig. 9(d) shows that breakdown occurs during the measurement of Sample 4D at 29.53 kV for an electric field of 3.45 kV/mm. The sample is sliced to determine the reason for the breakdown. The preimpregnated layer insulation is found to be glued to the electrodes, which has prevented the resin from flowing into the gap between the electrodes.

Two different types of PD patterns are recorded for Sample 5C. The first PD pattern (blue colored) that is recorded has a high magnitude at the first half-cycle and a low magnitude at the second half-cycle similar to Pattern-1, and the second PD pattern (orange colored) is a corona discharge pattern (Pattern-4) at the peak point of the negative cycle, as shown in Fig. 9(e).

Samples 8B and 11B show PDs with shapes similar to that of Pattern-1, as shown in Fig. 9(f) and (j).

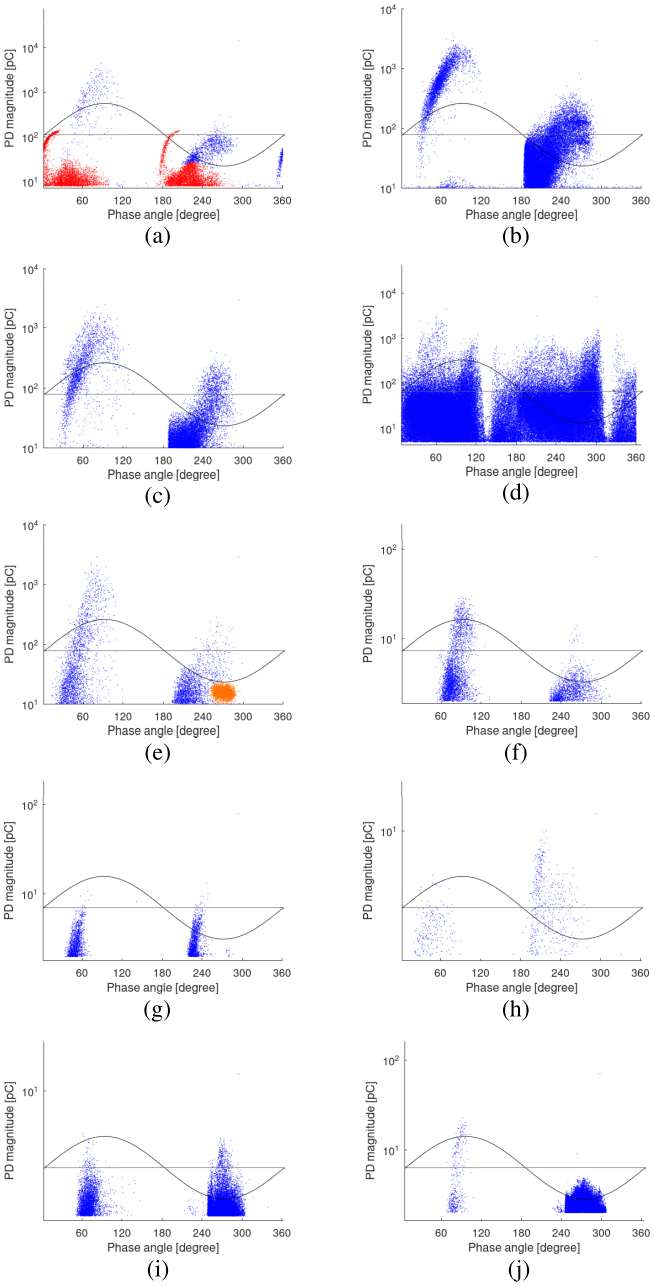

Fig. 9. PD patterns of Type-2 samples. (a) PD for Sample 3B (Patterns-1 and 3). (b) PD for Sample 4B (Pattern-1). (c) PD for Sample 4C (Pattern-1). (d) PD for Sample 4D (Breakdown). (e) PD for Sample 5C (Patterns-1 and 4). (f) PD for Sample 8B (Pattern-1). (g) PD for Sample 9A (Pattern-2). (h) PD for Sample 9B (Pattern-2). (i) PD for Sample 11A (Pattern-2). (j) PD for Sample 11B (Pattern-1).

The PD patterns of Samples 9A, 9B, and 11A have similar magnitudes and densities at both the half-cycles of the applied voltage and are similar to Pattern-2.

No PD event is recorded for Samples 6B, 6D, 8A, and 10A for electric fields up to 3.55, 3.32, 2.75, and 3.4 kV/mm, respectively.

The analysis results for the Type-2 samples are presented in Table VII, where V_{inc}, PD_{max}, and E_{sim} denote the measured PD inception voltage, the measured maximum PD magnitude at V_{inc}, and the maximum electric field intensity finding from the simulation study at V_{inc}, respectively. During the test, the applied voltage is increased by 100-V steps per second, and the magnitude of the initial voltage of the PD is taken as V_{inc}.

TABLE VII
ANALYSIS RESULTS FOR TYPE-2 SAMPLES

Sample	V_{inc} (kV)	PD_{max} (pC)	PD pattern	E_{sim} (kV/mm)
3B	30.53	3400	Pattern-1	2.8
3B	25.02	154	Pattern-3	-
4B	25.04	2400	Pattern-1	2.92
4C	25.24	1600	Pattern-1	2.99
4D	29.53	4452	Breakdown	3.45
5C	21.28	738	Pattern-1	3.18
5C	22.05	25	Pattern-4	-
6B	30	None	None	up to 3.55
6D	30	None	None	up to 3.32
8A	36	None	None	up to 2.75
8B	33	10	Pattern-1	3.7
9A	23.84	10.22	Pattern-2	3.34
9B	33.55	17.23	Pattern-2	4.85
10A	36	None	None	up to 3.4
11A	31.59	5.6	Pattern-2	4.07
11B	36	17.9	Pattern-1	4.4

For Patterns-3 and 4, the electric field cannot be simulated because the sources of these patterns lie outside the insulation materials.

C. Samples With Conductors (Type-3)

The recorded PD patterns of the Type-3 samples are shown in Fig. 10.

Fig. 10(a) and (b) show a low-density high-amplitude PD (blue colored) at the positive cycle and a high-density low-amplitude PD (blue colored) at the negative cycle similar to Pattern-1 for Samples 3A and 3C. On the other hand, Fig. 10(e) shows a high-density low-amplitude PD at the positive cycle and a low-density high-amplitude PD at the negative cycle similar to Pattern-1 for Sample 8D. These patterns show that voids are closed to the voltage applied conductor in Samples 3A and 3C and closed to the grounded conductor in Sample 8D.

Fig. 10(b) shows that the PD pattern (orange colored) for Sample 3C has a shape similar to the corona of Pattern-4 at the negative peak voltage.

The PD pattern (red colored) of Samples 3A, 3C, and 3D exhibits a zero-crossing of the applied voltage, similar to Pattern-3. Unlike Pattern-3, the maximum PD magnitude does not remain constant as the phase angle varies. However, the PD events start at the same time, where all the PD events shown in red color are considered to result from the same PD source.

The PD pattern of Samples 8C has similar magnitudes and densities at both the half-cycles of the applied voltage and is similar to Pattern-2 as shown in Fig. 10(d).

The analysis results for the Type-3 samples are presented in Table VIII.

D. Samples With Conductor and Layer Insulation (Type-4)

The recorded PD patterns of the Type-4 samples are shown in Fig. 11. No PD event is recorded for Sample 6C for electric fields up to 11 kV/mm.

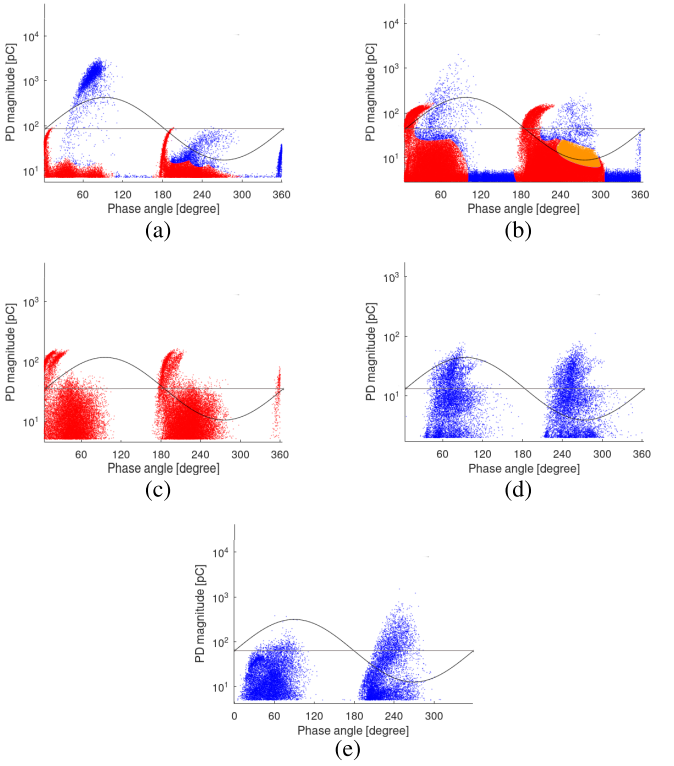

Fig. 10. PD patterns of Type-3 samples. (a) PD for Sample 3A (Patterns-1 and 3). (b) PD for Sample 3C (Patterns-1, 3, and 4). (c) PD for Sample 3D (Pattern-3). (d) PD for Sample 8C (Pattern-2). (e) PD for Sample 8D (Pattern-1).

TABLE VIII
ANALYSIS RESULTS FOR TYPE-3 SAMPLES

Sample	V_{inc} (kV)	PD_{max} (pC)	PD pattern	E_{sim} (kV/mm)
3A	28.7	1504	Pattern-1	7.5
3A	29.02	120	Pattern-3	-
3C	26.8	1650	Pattern-1	5.4
3C	24.77	152	Pattern-3	-
3C	27.36	30	Pattern-4	-
3D	25.57	158	Pattern-3	-
8C	33.54	3.5	Pattern-2	7.154
8D	31.64	8.36	Pattern-1	6.37

The PD patterns for all other samples have similar magnitudes and densities at both the half-cycles of the applied voltage and are similar to Pattern-2. However, an additional pattern is recorded for Sample 5A that is similar to Pattern-1, which is shown in pink color in Fig. 11(a).

The analysis results for the Type-4 samples are presented in Table IX, where [1] and [2] denote the electric fields in the conductor insulation and fiberglass mesh, respectively. The electrical field of conductor insulation for samples containing conductor C4, which is a noninsulated conductor, is shown as NA in the table.

VII. DISCUSSION

PD source causing Patterns-1 and 2 during tests is due to the void in the insulation material. Bad contact or corona patterns are related to test setups, and PD sources of these situations are unknown positions outside the samples. Therefore, only the results associated with Patterns-1 and 2 are discussed in this section.

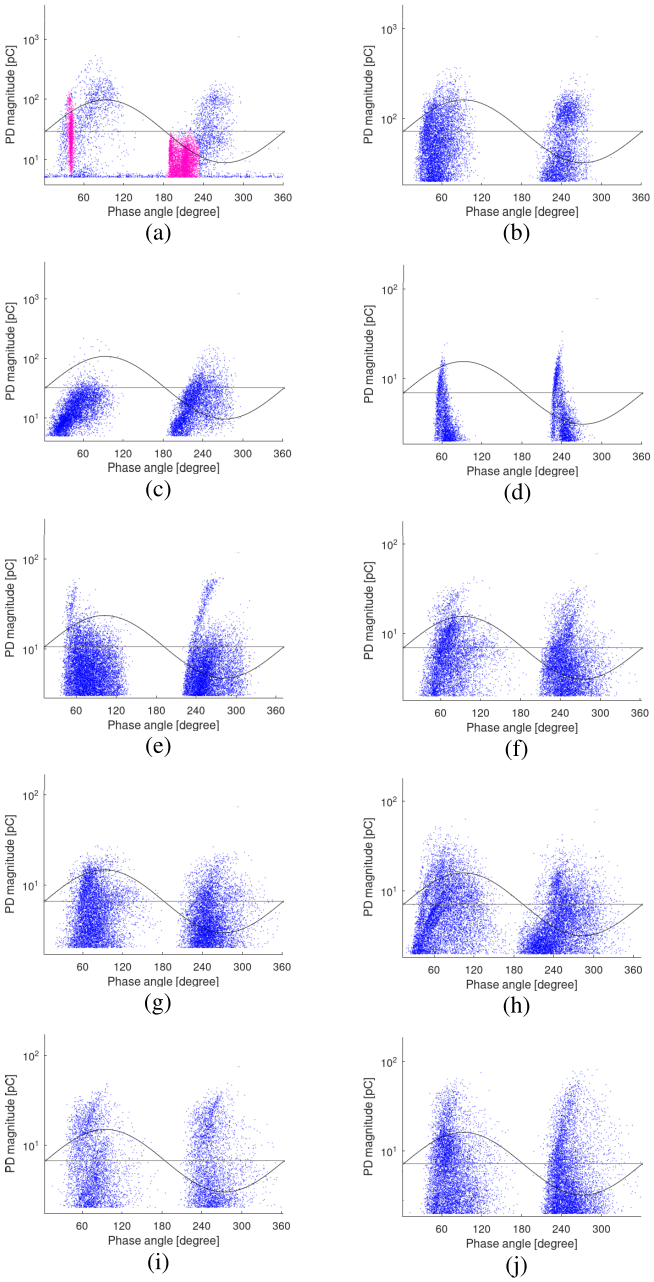

Fig. 11. PD patterns of Type-4 samples. (a) PD for Sample 5A (Patterns-1 and 2). (b) PD for Sample 5B (Pattern-2). (c) PD for Sample 5D (Pattern-2). (d) PD for Sample 7A (Pattern-2). (e) PD for Sample 7B (Pattern-2). (f) PD for Sample 9C (Pattern-2). (g) PD for Sample 9D (Pattern-2). (h) PD for Sample 10D (Pattern-2). (i) PD for Sample 11C (Pattern-2). (j) PD for Sample 11D (Pattern-2).

The insulation material results are presented in a group of L1–L4, L3, and L5–L6 which are used in a similar location in MV windings of the CRDT.

Fig. 12 shows that the samples containing L1 layer insulation have the lowest PD inception electric field. L1 shows similar characteristics for electric fields from 2.36 to 4.85 kV/mm for all the samples. This result could be attributed to the three-ply structure of L1. The L1 layers are attached with glue,

TABLE IX
ANALYSIS RESULTS FOR TYPE-4 SAMPLES

Sample	V_{inc} (kV)	PD_{max} (pC)	PD pattern	E_{sim} (kV/mm)
5A	29.5	192	Pattern- 2(blue)	5.05[1] & 2.5[2]
5A	31.2	112	Pattern-1(pink)	5.05[1] & 2.5[2]
5B	21.42	185	Pattern-2	7.47[1] & 4.49[2]
5D	20.5	52	Pattern-2	4.47[1] & 2.51[2]
6C	30	None	None	NA[1] & up to 11[2]
7A	12.24	19.08	Pattern-2	NA[1] & 4.62[2]
7B	10.97	31.76	Pattern-2	NA[1] & 3.99[2]
9C	25.34	13.87	Pattern-2	6.51[1] & 3.59[2]
9D	23.19	7.6	Pattern-2	4.65[1] & 2.36[2]
10D	13.66	60.07	Pattern-2	NA[1] & 5.25[2]
11C	24.95	18.36	Pattern-2	7.22[1] & 4.36[2]
11D	18.88	27.61	Pattern-2	5.77[1] & 3.32[2]

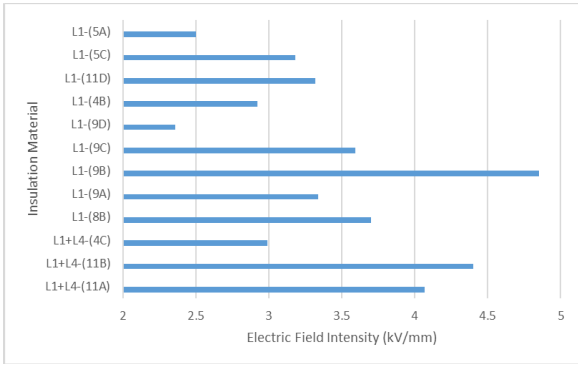

Fig. 12. Electric field intensity in L1 and L1 + L4 insulation materials.

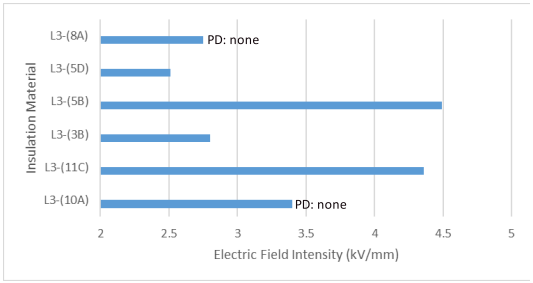

Fig. 13. Electric field intensity in L3 insulation materials.

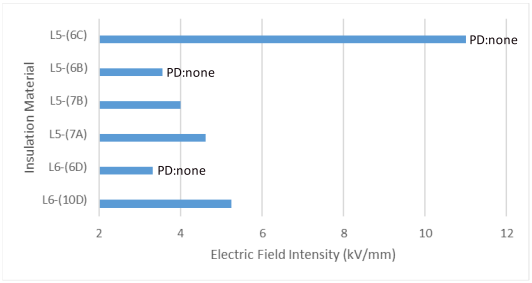

Fig. 14. Electric field intensity in L5 and L6 insulation materials.

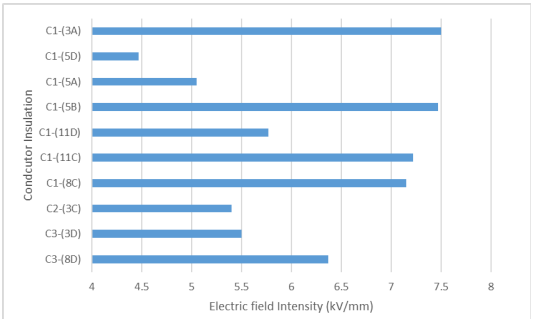

Fig. 15. Electric field intensity in conductor insulations.

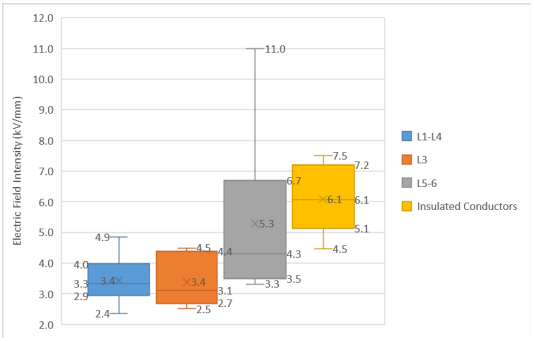

Fig. 16. Summary of electric field intensity for material groups.

which may not be uniformly distributed between each layer. Any space without glue may cause PD, or a high electric field may delaminate the material at the point where the glue is weakly attached.

The electric fields are similar for the samples containing L1 and L1 + L4. Therefore, the L4 polyester tape does not appear to have a significant effect on the results.

Fig. 13 shows that the inception electric field of PD differs among the L3 samples. This result may be attributed to the material structure. L3 is woven with fiberglass strings into a shape with large rectangular holes, followed by resin impregnation and curing. Voids are introduced into L3 during production. The resin may not fill some voids during casting of the winding containing L3, and these voids may cause PD.

L5 and L6 are one-ply insulation films. Recorded PD events start at 3.99 kV/mm of the electric field which is higher than other insulation materials as shown in Fig. 14.

Fig. 15 shows that the insulated conductors have a higher PD inception electric field than the insulation materials. The conductors are covered by a polyester film, followed by wrapping with fiberglass strings, varnishing, and drying. Enamel insulation is applied to conductors under a vacuum. These processes prevent the formation of large voids in the vicinity of the metallic components of the conductor and may increase the inception electric field for PD.

A box graph of each material group is given in Fig. 16 for general view.

In this study, voids or cracks are not modeled. The size and location of voids cannot be known during the design stage. In addition, the electric field in these voids or cracks may be higher than the insulation medium. But designers may limit the electric field in the desired insulation material following this study not to have PD in equipment.

These results are based on the quality of the casting oven and used materials in the BEST Transformer Company and may differ in other facilities which do not have good casting

ovens or materials. In addition, the background noise of the measurement system with a voltage source can reach 3 pC of the PD level. The mentioned results are obtained with up to 3 pC of background noise, and any PD event less than 3 pC is ignored.

VIII. Conclusion

In this study, PD is measured for 40 samples that are fabricated with four different insulation structures corresponding to the MV winding of the CRDT made by the BEST Transformer Company. All the samples are tested, and finite element software is used to simulate models of these samples. Eleven different types of materials, such as epoxy resin, three-ply insulation, fiberglass mesh, polyester film, polyimide film, enamel, and fiberglass insulated round and rectangular conductors, are used to fabricate the four types of samples. The PD inception voltage and PD inception electric field of all the samples are obtained. The following conclusions are drawn from the results of the study.

1) A pure resin mix that is not combined with other insulation materials does not contain voids that cause PD detectable by a PD measurement system.
2) Most of the recorded PD pattern types are Pattern-1. The high electric field in the vicinity of the electrode or conductor may result in delamination of the insulation material or conductor insulation very close to the conductor. In addition, an air bubble may be trapped between the conductor part and the insulation material during resin casting depending on the surface roughness of a material.
3) PD inception occurs for electric fields from 2.36 to 4.85 kV/mm in three-ply laminated insulation materials inside a cast-resin block.
4) Fiberglass meshes have various inception electric fields because of the quality of the production process.
5) Insulated conductors have a very high PD inception electric field because of the production process of these conductors.
6) Insulated conductors and epoxy resin are reliable materials. However, the maximum electric field in a winding should not exceed 2.99 kV/mm for three-ply glued insulation material or 2.7 kV/mm for fiberglass meshes to stay on the 75% safe side to ensure the transformer is PD-free. The susceptibility to PD can be improved using one-ply polyester or polyimide materials instead of three-ply materials.

Future work will focus on the PD behavior of those materials after aging.

References

[1] M. Erdogan and M. K. Eker, "Analysis of lightning impulse voltage distribution for a dry-type transformer using three different winding types," *Electr. Power Syst. Res.*, vol. 188, Nov. 2020, Art. no. 106527.

[2] W. Y. Chang, "Application of fuzzy C-means clustering approach and genetic algorithm to partial discharge pattern recognition," *Int. Rev. Electr. Eng.*, vol. 7, no. 4, pp. 5213–5220, 2012.

[3] R. Kotte, E. Gockenbach, and H. Borsi, "Influence of the cure parameters on the partial discharge behavior of cast resins," in *Proc. Conf. Rec. IEEE Int. Symp. Electr. Insul.*, Apr. 2002, pp. 387–390.

[4] D. Muto, M. Oya, T. Aoi, and T. Ueno, "A study on partial discharge phenomena of winding wires," *Furukawa Rev.*, vol. 45, pp. 13–21, Mar. 2014.

[5] T. Ozaki, T. Imai, F. Sawa, T. Shimizu, and F. Kanemitsu, "Partial discharge resistant enameled wire," in *Proc. Int. Symp. Electr. Insulating Mater. (ISEIM)*, vol. 1, Jun. 2005, pp. 184–187.

[6] W. A. Izzati, Y. Z. Arief, Z. Adzis, and M. Shafanizam, "Partial discharge characteristics of polymer nanocomposite materials in electrical insulation: A review of sample preparation techniques, analysis methods, potential applications, and future trends," *Sci. World J.*, vol. 2014, pp. 1–14, Jan. 2014.

[7] N. M. K. Abdel-Gawad, A. Z. El Dein, D.-E.-A. Mansour, H. M. Ahmed, M. M. F. Darwish, and M. Lehtonen, "Experimental measurements of partial discharge activity within LDPE/TiO_2 nanocomposites," in *Proc. 19th Int. Middle East Power Syst. Conf. (MEPCON)*, Dec. 2017, pp. 811–816.

[8] H. A. Awan, S. Amin, T. U. Rahman, U. Asad, and M. Awais, "Effect of regular and core shell nano fillers on the partial discharge and tracking performance of low density polyethylene," *Mater. Res. Exp.*, vol. 7, no. 1, Jan. 2020, Art. no. 015062.

[9] Y. Zhao, G. Zhang, D. Han, K. Li, Z. Qiu, and F. Yang, "Experimental study on the insulation properties of epoxy casting resins under high-frequency square waveform," *CSEE J. Power Energy Syst.*, vol. 7, no. 99, pp. 1–10, 2019.

[10] J. Song, J. Zhu, M. Tian, S. Zhang, and M. Wen, "Investigation on the partial discharge of the cavity in nomex insulation for mining dry type transformer," *Gaodianya Jishu/High Voltage Eng.*, vol. 44, no. 12, pp. 4071–4082, 2018.

[11] H. Moranda, H. Moscicka-Grzesiak, P. Przybylek, K. Walczak, and R. Szewczyk, "Comparative tests of partial discharges in Nomex 910 paper and cellulose paper," *Energies*, vol. 13, no. 3, pp. 2–9, 2020.

[12] M. Florkowski, B. Florkowska, M. Kuniewski, and P. Zydron, "Comparison of effective discharge area in voids in different insulating materials based on surface resistance," in *Proc. 21st Int. Symp. High Voltage Eng.*, B. Németh, Ed. Cham, Switzerland: Springer, 2020, pp. 22–31.

[13] Y. Wang, Y. Luo, J. Guan, and R. Ding, "Dielectric properties of epoxy resin impregnated paper insulation in different stages of partial discharge development," *Polym. Compos.*, vol. 41, no. 1, pp. 360–368, Jan. 2020.

[14] B. Song, M. Ren, Z. Zhang, T. Zhuang, C. Zhang, and M. Dong, "Excess conduction induced by partial discharge in polymer," *J. Phys. D, Appl. Phys.*, vol. 53, no. 48, Nov. 2020, Art. no. 485302.

[15] Y. Wang, C. Feng, R. Fei, and Y. Luo, "Thermal-ageing characteristics of dry-type transformer epoxy composite insulation," *High Perform. Polym.*, vol. 32, no. 7, pp. 741–752, Sep. 2020.

[16] *Power Transformers—Part 11: Dry-Type Transformers*, Standard IEC 60076–11, 2018.

[17] *IEEE Standard for General Requirements for Dry-Type Distribution and Power Transformers*, Standard C57.12.01, IEEE, 2015.

[18] (2019). Omicron. *MPD 600*. [Online]. Available: https://www.omicronenergy.com/download/document/1A409BBD-B3A3-4A36-ACDD-1B86D10C1C11/

[19] N. M. K. Abdel-Gawad, A. Z. El Dein, D. A. Mansour, H. M. Ahmed, M. M. F. Darwish, and M. Lehtonen, "Development of industrial scale PVC nanocomposites with comprehensive enhancement in dielectric properties," *IET Sci., Meas. Technol.*, vol. 13, no. 1, pp. 90–96, Jan. 2019.

[20] (1969). CIGRE WG 21.03. TC21. *Recognition of Discharges*. Electra. [Online]. Available: https://e-cigre.org/publication/ELT_011_2-recognition-of-discharges

[21] H. Illias, T. Soon Yuan, A. H. A. Bakar, H. Mokhlis, G. Chen, and P. L. Lewin, "Partial discharge patterns in high voltage insulation," in *Proc. IEEE Int. Conf. Power Energy (PECon)*, Dec. 2012, pp. 750–755.

[22] H. Odoglu, *Transformatör ve sönt Reaktör Deneyleri*, 2nd ed. Ankara, Turkey: Chamber of Electrical Engineers, 2013.

[23] A. Carlson, J. Fuhr, G. Schemel, and F. Wagscheider, *Testing Power Transformers*, 2003rd ed. Dusseldorf, Germany: ProPrint GmbH, 2000.